

# Josephson Diode Effect Induced by Valley Polarization in Twisted Bilayer Graphene

Jin-Xin Hu<sup>1</sup>,\* Zi-Ting Sun<sup>1</sup>,\* Ying-Ming Xie,<sup>†</sup> and K. T. Law<sup>‡</sup>

*Department of Physics, Hong Kong University of Science and Technology, Clear Water Bay, Hong Kong, China*



(Received 5 December 2022; accepted 26 May 2023; published 30 June 2023)

Recently, the Josephson diode effect (JDE), in which the superconducting critical current magnitudes differ when the currents flow in opposite directions, has attracted great interest. In particular, it was demonstrated that gate-defined Josephson junctions based on magic-angle twisted bilayer graphene showed a strong nonreciprocal effect when the weak-link region is gated to a correlated insulating state at half filling (two holes per moiré cell). However, the mechanism behind such a phenomenon is not yet understood. In this Letter, we show that the interaction-driven valley polarization, together with the trigonal warping of the Fermi surface, induce the JDE. The valley polarization, which lifts the degeneracy of the states in the two valleys, induces a relative phase difference between the first and the second harmonics of the supercurrent and results in the JDE. We further show that the nontrivial current phase relation, which is responsible for the JDE, also generates the asymmetric Shapiro steps.

DOI: 10.1103/PhysRevLett.130.266003

**Introduction.**—Supercurrents flow through a junction formed by two superconductors connected by a weak link, which are called Josephson junctions (JJs) [1–4]. Symmetry breaking plays a key role in the properties of JJs. For example,  $\pi$  JJs can be formed when the time-reversal symmetry is broken, which exhibit a phase difference of  $\pi$  for the two superconductors in the ground state [5–8]. When both time-reversal and inversion symmetry are broken, JJs can show the Josephson diode effect (JDE) [9–15], in which the critical supercurrent  $|I_c|$  is nonreciprocal in the sense that  $|I_{c+}|$  for the current flowing in the “+” direction is different from  $|I_{c-}|$  for the opposite “–” direction. Such nonreciprocity in supercurrents could have potential applications in superconducting electronics [16–18]. Recently, there has been worldwide interest in exploring the JDE in various systems, such as in NbSe<sub>2</sub>/Nb<sub>3</sub>Br<sub>8</sub>/NbSe<sub>2</sub> heterostructures [19], topological semimetals [20], and gated-defined JJs in twisted bilayer graphene (TBG) [21].

The observation of JDE in gated-defined JJs based on TBG is particularly interesting [21]. In the experiment, a single piece of magic-angle TBG was gated into three different regions to form a superconductor–correlated insulator–superconductor JJ as depicted in Fig. 1(a). When the correlated insulating state is at half filling (two holes per moiré unit cell), a large JDE was observed. It is important to note that current theories of JDE [9,10,12–14] require the presence of spin-orbit coupling, but the spin-orbit coupling is negligible in TBG. Moreover, external in-plane magnetic fields were required to induce JDE in other recent experiments [20,22]. It was proposed that the in-plane magnetic field induces finite-momentum Cooper pairing at the surface of the superconductors, which is essential for explaining the JDE [11]. On the other hand, in

gate-defined JJ in TBG, time-reversal symmetry is broken spontaneously at the weak-link region by interactions and there is no evidence of finite-momentum pairing in the superconducting regions. Therefore, a new microscopic theory is needed to understand this interaction-driven JDE in TBG.

In this Letter, we show that the interaction-driven valley-polarization order parameter at the weak-link region [Fig. 1(a)], as well as the trigonal warping of the Fermi surface [Fig. 3(b)] play essential roles in inducing the JDE. In the following sections, we first introduce a continuum model describing the gate-defined JJ with a valley-polarized state as the weak link. In the one-dimensional (1D) limit, we show analytically how the valley polarization together with the trigonal warping of the Fermi surface induce a relative phase difference between the first and the second harmonics of the Josephson current as shown in Eq. (6). This nontrivial current-phase relation (CPR) gives rise to JDE. Second, we illustrate the JDE for magic-angle

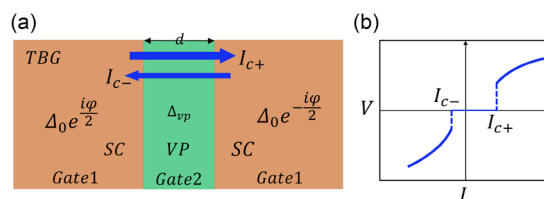


FIG. 1. (a) A schematic picture of a gate-defined JJ based on magic-angle TBG. The left (right) side of the junction is superconducting (SC) with pairing order parameter  $\Delta_0 e^{\pm i\phi/2}$ , respectively. The weak-link region is an interaction-driven valley-polarized (VP) state with width  $d$ . (b) A schematic illustration of the  $V-I$  curve of a JJ with asymmetric critical currents  $|I_{c+}| \neq |I_{c-}|$ , where  $V$  is the voltage across the JJ.

TBG numerically with a lattice model. Third, we show that gate-defined JJs would also exhibit asymmetric Shapiro steps (Fig. 4) which share the same origin as the JDE. Importantly, our theory can be generalized to JJs with magnetic field-driven spin polarization and it provides an alternative explanation of JDEs observed in other recent experiments [20,22,23].

*Continuum model.*—For magic-angle TBG with valley degrees of freedom with the interaction-induced valley polarization and trigonally warped Fermi surfaces, the low-energy effective Hamiltonian has the form [24,25]

$$H_{\tau}^{2D} = \lambda_0(k_x^2 + k_y^2) + \tau\lambda_1 k_x(k_x^2 - 3k_y^2) + \tau\Delta_{vp} - \mu, \quad (1)$$

where  $\tau = \pm 1$  is the valley index. The  $\lambda_0$  term is the kinetic energy, while the  $\lambda_1$  term denotes the trigonal warping effect, which breaks intravalley inversion symmetry such that  $H_{\tau}^{2D}(k_x) \neq H_{\tau}^{2D}(-k_x)$ . The time-reversal symmetry is also broken by the valley polarization  $\Delta_{vp}$ . For simplicity, we first take  $k_y = 0$ , such that

$$h_{\tau} = \lambda_0 k_x^2 + \tau\lambda_1 k_x^3 + \tau\Delta_{vp} - \mu. \quad (2)$$

This effective 1D model allows the key results to be calculated analytically and the properties of the two-dimensional system will be demonstrated using a lattice model numerically in a later section.

In Fig. 2(a), a schematic figure of a 1D superconductor–valley-polarized state–superconductor (SC-VP-SC) JJ is shown, where  $\varphi$  is the phase difference between the two superconductors. We assume that the pairing in the superconducting regions are conventional *s*-wave pairing, and the weak-link region is a valley-polarized state ( $\Delta_{vp}$  is finite, which breaks the degeneracy of the two valleys). The energy bands of  $h_{\tau}$  are shown in Fig. 2(b). As Andreev reflections only involve electrons near the Fermi surface, we can make the Andreev approximation to linearize the dispersion relations in the vicinity of the Fermi momentum, and the full junction can be described by the Bogoliubov–de Gennes Hamiltonian in the Nambu basis as  $[\psi_{\tau\alpha}(x), \psi_{-\tau,-\alpha}^{\dagger}(x)]^T$ ,

$$\hat{H}_{\alpha}^{\tau} = \begin{pmatrix} \hat{h}_{\tau,\alpha}(x) & \Delta_s(x) \\ \Delta_s^*(x) & -\hat{h}_{-\tau,-\alpha}(x) \end{pmatrix}, \quad (3)$$

where  $\hat{h}_{\tau,\alpha}(x) = -i\hbar v_{\tau,\alpha}(x)\partial_x + \tau\Delta_{vp}(x)$ , and the Fermi velocity along the current direction is given by  $v_{\tau,\alpha}(x) = v_{s,\tau\alpha}[\Theta(-x) + \Theta(x-d)] + v_{vp,\tau\alpha}\Theta(x)\Theta(d-x)$ , where  $v_{s,\tau\alpha}$  and  $v_{vp,\tau\alpha}$  are the Fermi velocities for the superconducting and the valley-polarized regions, respectively. Here,  $\alpha = \pm 1$  denote the right and left movers of the electrons. The slopes of the black arrows in Fig. 2(b) indicate the Fermi velocities of the left and right movers schematically. Notably, the trigonal warping term that breaks the

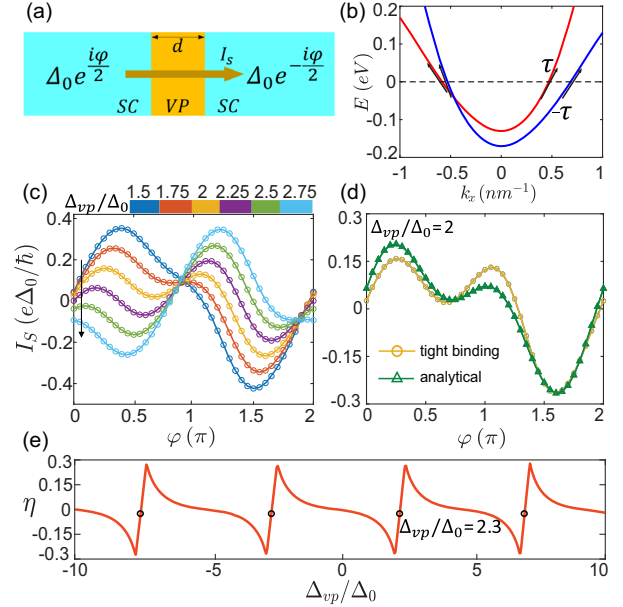


FIG. 2. (a) Schematic illustration of a 1D JJ. The left (right) side of the junction is a conventional superconductor with order parameter  $\Delta_0 e^{+(-)i\varphi/2}$ . The weak-link region is valley polarized with width  $d$ . (b) The band structure of the weak-link region with valley-polarization order parameter  $\Delta_{vp} = 20$  meV. The slopes of the black arrows indicate the amplitudes of the Fermi velocities at the Fermi energy. (c) The Josephson CPR  $I_s$  for  $\Delta_{vp}/\Delta_0$  going from 1.5 to 2.75. As  $\Delta_{vp}/\Delta_0$  increases (indicated by the black arrow),  $\partial I_s/\partial\varphi$  at  $\varphi = 0^+$  changes sign. (d) The tight binding (yellow circle) and analytical (green triangle) calculations of  $I_s$  for  $\Delta_{vp}/\Delta_0 = 2$ . (e) The nonreciprocity efficiency  $\eta$  as a function of  $\Delta_{vp}/\Delta_0$ . The  $0-\pi$  transition points are labeled by black circles. The temperature is set to be  $k_B T = 0.2\Delta_0$ .

intravalley inversion symmetry leads to  $v_{vp,\tau+} \neq -v_{vp,\tau-}$ . To describe the SC-VP-SC junction, the superconducting order parameter is set to be  $\Delta_s(x) = \Delta_0[e^{i\varphi/2}\Theta(-x) + e^{-i\varphi/2}\Theta(x-d)]$ , and the valley-polarization order parameter is  $\Delta_{vp}(x) = \Delta_{vp}\Theta(x)\Theta(d-x)$ . In the calculations for Fig. 2, model parameters are  $\lambda_0 = 0.5$  eV nm<sup>2</sup>,  $\lambda_1 = 0.2$  eV nm<sup>3</sup>,  $\mu = 0.15$  eV,  $\Delta_0 = 4$  meV, and  $d = 40$  nm.

*Nonreciprocal CPR.*—A lattice model of Eq. (2) is established in the Supplemental Material [26], and the Josephson supercurrent  $I_s$  passing through the JJ with different  $\Delta_{vp}$  are calculated [26] and shown in Fig. 2(c). It is interesting to note that, as  $\Delta_{vp}/\Delta_0$  increases (say, from 1.5 to 2.75),  $\partial I_s/\partial\varphi$  at  $\varphi = 0^+$  changes sign. As a result, the CPR of  $I_s$  as a function of  $\varphi$  changes from  $I_s \approx \sin\varphi$  to  $I_s \approx \sin(\varphi + \pi)$ . In another words, there is a  $0$  to  $\pi$ -junction transition as  $\Delta_{vp}$  increases. Importantly, near the  $0-\pi$  transition, the critical (or the maximum) supercurrent flowing in the positive direction  $I_{c+}$  differs from the critical supercurrent  $I_{c-}$  flowing in the negative direction. The nonreciprocity efficiency  $\eta = (I_{c+} - |I_{c-}|)/(I_{c+} + |I_{c-}|)$  can be as large as 30% at  $\Delta_{vp}/\Delta_0 = 2$  [yellow circle

line in Fig. 2(c)]. In other words, the JJ with valley polarization and the trigonal warping term shows a significant JDE near the  $0-\pi$  transition.

In the remainder of this section, we present an analytical description of JDE. To calculate the Josephson current, we use [35]

$$I_s(\varphi) = -\frac{4e}{\hbar\beta} \frac{d}{d\varphi} \sum_{n=0}^{\infty} \text{In det}[1 - S_A(i\omega_n, \varphi)S_N(i\omega_n, \varphi)], \quad (4)$$

where  $\beta = 1/k_B T$ ,  $T$  is the temperature, and the Matsubara frequencies  $\omega_n = (2n + 1)\pi/\beta$ .  $S_A$  and  $S_N$  are the scattering matrices of the junction for the Andreev reflection and the normal scattering processes, respectively. As shown in the Supplemental Material [26], we find that the  $0-\pi$  transitions occur at

$$\frac{2\Delta_{\text{vp}}}{E_T} = \left(m + \frac{1}{2}\right)\pi, \quad m \in \mathbb{Z}. \quad (5)$$

Here,  $E_T$  is the Thouless energy measuring the bandwidth, which is defined as  $E_T = \hbar\bar{v}_{\text{vp}}/d$ , and  $\bar{v}_{\text{vp}} = 2/(v_{\text{vp},++}^{-1} + v_{\text{vp},--}^{-1})$ . Note that  $v_{\text{vp},\tau\alpha}$  are the Fermi velocities of the valley-polarized region at valley  $\tau$  and moving in the  $\alpha$  directions. Near the zeroth  $0-\pi$  transition point where  $m = 0$ , we find that the CPR from Eq. (4) can be approximately written as [26]

$$I_s(\varphi) = I_1 \sin(\tilde{\varphi} + \delta) + I_2 \sin(2\tilde{\varphi}), \quad (6)$$

with  $\tilde{\varphi} = \varphi - \Delta_{\text{vp}}/E_A$ . The coefficients  $I_1$ ,  $I_2$ , and  $\delta$  are

$$I_1 = -\frac{16e \cosh \delta_T}{\hbar\beta(1 + 2\sinh^2 \delta_T)} \left(\frac{2\Delta_{\text{vp}}}{E_T} - \frac{\pi}{2}\right), \quad (7)$$

$$I_2 = \frac{8e \text{sech}^2 \delta_A}{\hbar\beta(1 + 2\sinh^2 \delta_T)}, \quad (8)$$

$$\delta = -\arctan \left[ \tanh \delta_A \tanh \delta_T \left/ \left(\frac{2\Delta_{\text{vp}}}{E_T} - \frac{\pi}{2}\right) \right. \right]. \quad (9)$$

Here,  $\delta_A = \pi E_A^{-1}/\beta$  and  $\delta_T = 2\pi(\Delta_0^{-1} + E_T^{-1})/\beta$ .  $E_A = \hbar\delta\bar{v}_{\text{vp}}/d$  is the energy scale that reveals the intravalley inversion breaking, where  $\delta\bar{v}_{\text{vp}}$  is defined as  $\delta\bar{v}_{\text{vp}} = 1/(v_{\text{vp},++}^{-1} - v_{\text{vp},--}^{-1})$ . For Eq. (7), it is clear that  $I_1$  changes sign when  $\Delta_{\text{vp}}$  increases such that  $2\Delta_{\text{vp}}/E_T > \pi/2$ . As a result, the phase of the first harmonic acquires a phase change of  $\pi$  which causes the  $0-\pi$  transition. Interestingly, at higher temperatures,  $I_2$  gets suppressed and  $I_s$  conforms to a sinusoidal function such that  $I_s \approx \sin(\varphi + \varphi_0)$ . The anomalous phase  $\varphi_0 = -\Delta_{\text{vp}}/E_A$  is the phase shift induced by the valley polarization. More importantly,  $\delta$  in Eq. (9), which is the relative phase difference between the first and the second harmonic Josephson currents, induced by the

valley polarization and the trigonal warping term, would result in the JDE. As shown in Fig. 2(d), the analytical results of the Josephson current from Eqs. (6)–(9) match the results of the tight binding calculations very well. It is clear from Fig. 2(d) that there is a large difference between  $I_{c+}$  and  $I_{c-}$  and thus a large JDE. This is the central result of this Letter.

Furthermore, the nonreciprocity efficiency  $\eta$  as a function of  $\Delta_{\text{vp}}$ , calculated using the 1D lattice model [26] is depicted in Fig. 2(e). It is interesting to note that  $\eta$  is a periodic function of  $\Delta_{\text{vp}}$  with the same periodicity as the  $0-\pi$  transitions. Near the  $0-\pi$  transitions,  $\eta$  is linearly proportional to  $\Delta_{\text{vp}} - \Delta_{\text{vp}}^m$ , where  $\Delta_{\text{vp}}^m = (m + 1/2)\pi E_T/2$ . This feature of  $\eta$  can be derived from the analytical results of Eq. (6).

*JDE in TBG.*—Experimentally, large JDE was observed in gated-defined JJs with magic-angle TBG [21] as schematically depicted in Fig. 1(a). However, the origin of the JDE is not yet known. The JDE was observed only when the weak-link region was gated to half filling (with two holes per moiré unit cell), and it is therefore the property of the weak link. In this section, we extend the 1D model calculations to 2D and show that the valley polarization [36–39] at half filling combined with trigonally warped Fermi surfaces naturally give rise to JDE in magic-angle TBG [21]. To capture the properties of the moiré bands in TBG, we use a lattice version of Eq. (1) [24,40]. The model can be written as

$$H_0^{\tau} = \sum_{\langle ij \rangle} t_1 c_{i\tau}^{\dagger} c_{j\tau} + \sum_{\langle ij \rangle'} (t_2 - it_2') c_{i\tau}^{\dagger} c_{j\tau} + \text{H.c.} \\ - \sum_i \mu_i c_{i\tau}^{\dagger} c_{i\tau}. \quad (10)$$

Here  $\langle ij \rangle$  denotes the first nearest hopping terms with amplitude  $t_1$ , and  $\langle ij \rangle'$  denotes the fifth nearest hopping terms with amplitudes  $t_2$  and  $t_2'$ , respectively. We set  $t_2 = 0.05t_1$  and  $t_2' = 0.2t_1$  in the following calculations. The annihilation operator of an electron with  $p_x + ip_y$  orbital on the site  $i$  is denoted by  $c_{i\tau}$ . For magic-angle TBG, the realistic bandwidth for lowest-energy moiré bands near charge neutrality is about 20 meV [41,42], which corresponds to  $t_1 = 4$  meV. The calculated band structure for the  $K$  and  $K'$  valleys is shown in Fig. 3(a). Also, the trigonally warped Fermi surfaces of TBG are shown in Fig. 3(b). The trigonal warping effect is characterized by  $t_2'$  [26].

In Fig. 1(a) we show a schematic picture of the gate-defined JJ of TBG with magic-angle TBG. For gate 1, the filling factor  $\nu$  is set to be  $\nu = -0.6$ , corresponding to the superconducting region [ $\mu = -8.7$  meV in Fig. 3(a)]. For gate 2,  $\nu$  is set to be  $\nu = -0.5$ , corresponding to the region of valley-polarized state [ $\mu = -7.2$  meV in Fig. 3(a)].

By introducing valley polarization  $\Delta_{\text{vp}}$ , we calculate  $I_s$  using the lattice Green's function approach [26] and the

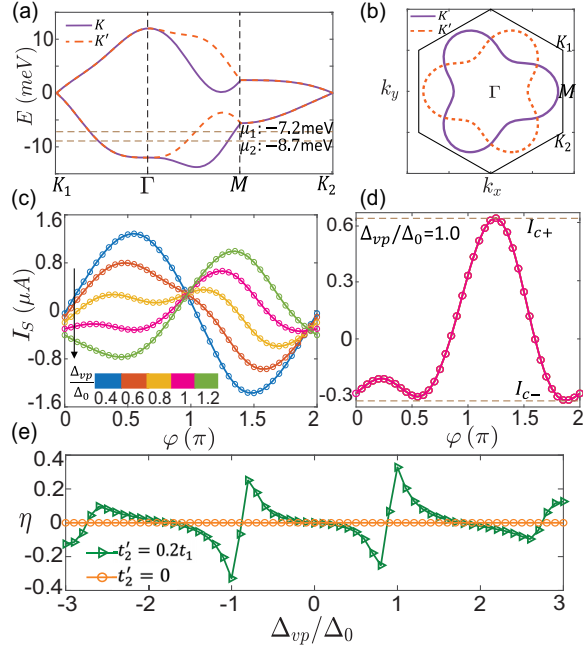


FIG. 3. (a) The energy bands of TBG calculated by the tight binding model. (b) The Fermi surfaces of  $K$  and  $K'$  valleys where the band filling  $\nu = -0.5$  [ $\mu = -7.2$  meV in (a)]. (c) The Josephson CPR  $I_s(\varphi)$  for  $\Delta_{vp}/\Delta_0$  going from 0.4 to 1.2 and a  $0-\pi$  transition is indicated by the black arrow. (d) The CPR with  $\Delta_{vp}/\Delta_0 = 1$  with  $\eta \approx 35\%$ . (e)  $\eta$  as a function of  $\Delta_{vp}/\Delta_0$  with (green triangle) and without (orange circle) warping term  $t'_2$ . The pairing potential  $\Delta_0 = 1.76k_B T_c \approx 0.4$  meV. The temperature is set to be  $k_B T = 0.15\Delta_0$ . The distance of the weak link is  $d = 6\sqrt{3}L_M$  and the width of the junction is  $W_J = 25L_M$ . The moiré lattice constant is  $L_M \approx 12.8$  nm.

results are shown in Fig. 3(c). As in the 1D case, there is a  $0-\pi$  transition as  $\Delta_{vp}$  increases and the zeroth  $0-\pi$  transition occurs at  $\Delta_{vp}/\Delta_0 \approx 0.9$ . At  $\Delta_{vp}/\Delta_0 \approx 1$ ,  $\eta$  is as large as 35% [Fig. 3(d)]. Moreover, in Fig. 3(e) we find that  $\eta$  depends sensitively on  $\Delta_{vp}$  and has the similar oscillatory behavior as in Fig. 2(e). Importantly, we notice that  $\eta$  is always zero as the warping term  $t'_2$  is turned off [Fig. 3(e)], which shows that the JDE in TBG further requires the intravalley inversion symmetry breaking by the trigonal warping effect on top of the time-reversal and inversion symmetry breaking. Interestingly, an additional spin-polarization order parameter can be added to the Hamiltonian and the JDE will only be changed quantitatively as shown in the Supplemental Material [26].

*Asymmetric Shapiro steps.*—In the sections above, we demonstrate that the unconventional CPR [Eq. (6)] induced by the valley polarization and the trigonal warping term give rise to JDE. In this section, we propose an alternative method for detecting the unconventional CPR of the SC-VP-SC JJ through the measurement of Shapiro steps [43,44]. This experiment can be conducted using a resistively shunted Josephson junction (RSJ) model, which is a

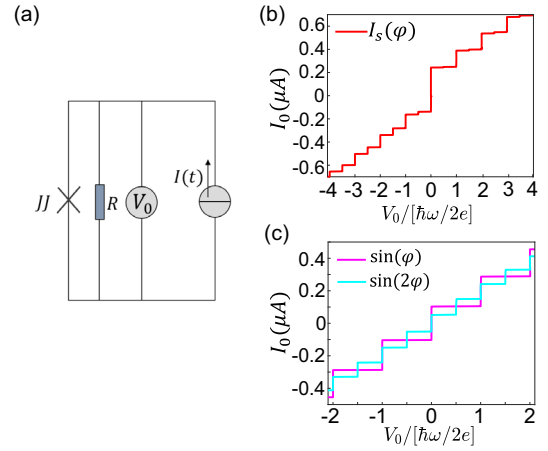


FIG. 4. (a) A schematic illustration of the Shapiro steps experiment. The RSJ is driven by the current  $I(t)$ , and the dc voltage  $V_0$  is measured. (b),(c) CVCs from the model illustrated in (a), with the dc  $I_0$  versus the dc voltage drop  $V_0$ . (b) The numerical result of CVCs, with typical parameters in laboratory  $\delta = \pi/3$ ,  $I_w = 0.8 \mu\text{A}$ ,  $R = 10\Omega$ ,  $\omega = 3.14$  GHz,  $I_1 = 0.2 \mu\text{A}$ ,  $I_2 = 0.8 \mu\text{A}$ . Shapiro steps appear at both integer and half-integer multiples of  $\hbar\omega/2e$ . An overall asymmetry  $I_0(V_0) \neq -I_0(-V_0)$  develops as the manifestation of the nonreciprocal nature. (c) Numerical results for  $\sin(\varphi)$  and  $\sin(2\varphi)$ , as comparisons.

circuit comprising a JJ in parallel with a resistance  $R$ . The current injected into the circuit consists of both the direct current (dc) and the alternating current (ac) components, namely,  $I(t) = I_0 + I_w \cos(\omega t)$ , and the dc voltage drop  $V_0$  can be measured as shown in Fig. 4(a). In the RSJ model, the phase dynamics follows [45]

$$I_0 + I_w \cos(\omega t) = V/R + I_s(\varphi), \quad (11)$$

where  $V$  is the overall voltage drop on the RSJ, which relates to the phase difference by the second Josephson equation  $d\varphi/dt = 2eV/\hbar$ ; the dc voltage drop  $V_0$  on the RSJ is just the time average of  $V$ , i.e.,  $V_0 = \langle V \rangle_T$ .

We numerically solved the RSJ equation with appropriate parameters for three different kinds of CPRs:  $I_s(\varphi)$  as given in Eq. (6) with finite  $I_1$ ,  $I_2$ , and  $\delta$ ,  $I_s(\varphi) \propto \sin(\varphi)$ , and  $I_s(\varphi) \propto \sin(2\varphi)$ . The resulting current-voltage characteristics (CVCs), in which the dc component  $I_0$  as a function of the dc voltage drop  $V_0$ , are plotted in Figs. 4(b) and 4(c). The current jumps of the Shapiro steps occur precisely when the dc voltage matches  $V_0 = k\hbar\omega/2e$ , as the integer Shapiro steps, or  $V_0 = k\hbar\omega/4e$ , as the half-integer Shapiro steps, where  $k = 0, \pm 1, \pm 2, \dots$ . We note that, near the  $0-\pi$  transition point, the second harmonic component dominates in the CPR, leading to a clear signature of the half-integer Shapiro steps [46]. Furthermore, compared to  $\sin(\varphi)$  and  $\sin(2\varphi)$ , the CVCs of nonreciprocal CPR  $I_s(\varphi)$  develops an overall asymmetric character  $I_0(V_0) \neq -I_0(-V_0)$  at both integer and half-integer Shapiro steps, as the manifestation of the nonreciprocal nature of the junction. A similar asymmetric CVC was also proposed

in a superconducting quantum-interference-device-based circuit very recently [47,48].

*Discussion.*—Recently, the study of the superconducting diode effect has attracted much attention both experimentally [16,49] and theoretically [50–53]. Most of the theories are based on magnetic-field-induced finite-momentum pairings. Some recent theories of the JDE also depend on the assumption of finite-momentum pairings in the bulk superconductor induced by magnetic fields. In this Letter, we show that the JDE can be generated by the weak link of the JJ alone.

We emphasize that the key ingredients for giving rise to the JDE here are the valley polarization and the trigonal warping effect. The pairing symmetries of the superconducting state and the details of the model Hamiltonian are not crucial. For example, it is shown in the Supplemental Material [26] that both the  $d$ -wave pairing and the  $p$ -wave pairing support the JDE in TBG. Regarding the model Hamiltonians, a five-band tight binding model of TBG [54] is used to calculate the JDE and the results are consistent with the results obtained using Eq. (10) [26].

Moreover, although our theory of JDE is based on electron-electron interaction-induced valley-polarized states in TBG with trigonal warping terms, our theory can be easily generalized to describe other materials, such as rhombohedral trilayer graphene [55,56] and Bernal-stacked bilayer graphene [57–59] which possess trigonal warping on the Fermi surface. We also expect our theory can apply to spin-polarized systems. In the Supplemental Material [26], we demonstrate the JDE for a Rashba wire with cubic spin-orbit coupling and an in-plane magnetic field that can be mapped to the valley-polarization problem with trigonal warping terms. The model is relevant to recent experiments in which two superconductors are connected by weak links with Rashba spin-orbit coupling and in-plane magnetic fields [20,22,23].

We thank Dima Efetov, Jaime Diez, Shuai Chen, and Adrian Po for inspiring discussions. K. T. L. acknowledges the support of the Ministry of Science and Technology, China, and Hong Kong Research Grant Council through Grants No. 2020YFA0309600, No. RFS2021-6S03, No. C6025-19G, No. AoE/P-701/20, No. 16310520, No. 16310219, No. 16307622, and No. 16309718. Y.-M. X. acknowledges the support of Hong Kong Research Grant Council through Grant No. PDFS2223-6S01.

\*J.-X. H. and Z.-T. S. contributed equally to this work.

†ymxie@ust.hk

‡phlaw@ust.hk

- [1] B. D. Josephson, *Phys. Lett.* **1**, 251 (1962).
- [2] B. Josephson, *Rev. Mod. Phys.* **36**, 216 (1964).
- [3] P. W. Anderson and J. M. Rowell, *Phys. Rev. Lett.* **10**, 230 (1963).
- [4] V. Ambegaokar and A. Baratoff, *Phys. Rev. Lett.* **10**, 486 (1963).
- [5] A. Feofanov, V. Oboznov, V. Bol’Ginov, J. Lisenfeld, S. Poletto, V. Ryazanov, A. Rossolenko, M. Khabipov, D. Balashov, A. Zorin *et al.*, *Nat. Phys.* **6**, 593 (2010).
- [6] T. Yamashita, K. Tanikawa, S. Takahashi, and S. Maekawa, *Phys. Rev. Lett.* **95**, 097001 (2005).
- [7] T. Kato, A. A. Golubov, and Y. Nakamura, *Phys. Rev. B* **76**, 172502 (2007).
- [8] T. Yamashita, S. Takahashi, and S. Maekawa, *Appl. Phys. Lett.* **88**, 132501 (2006).
- [9] F. Dolcini, M. Houzet, and J. S. Meyer, *Phys. Rev. B* **92**, 035428 (2015).
- [10] C.-Z. Chen, J. J. He, M. N. Ali, G.-H. Lee, K. C. Fong, and K. T. Law, *Phys. Rev. B* **98**, 075430 (2018).
- [11] M. Davydova, S. Prembabu, and L. Fu, *Sci. Adv.* **8**, eabo0309 (2022).
- [12] Y. Zhang, Y. Gu, P. Li, J. Hu, and K. Jiang, *Phys. Rev. X* **12**, 041013 (2022).
- [13] Y. Tanaka, B. Lu, and N. Nagaosa, *Phys. Rev. B* **106**, 214524 (2022).
- [14] B. Lu, S. Ikegaya, P. Bursset, Y. Tanaka, and N. Nagaosa, *arXiv:2211.10572*.
- [15] D. Wang, Q.-H. Wang, and C. Wu, *arXiv:2209.12646*.
- [16] F. Ando, Y. Miyasaka, T. Li, J. Ishizuka, T. Arakawa, Y. Shiota, T. Moriyama, Y. Yanase, and T. Ono, *Nature (London)* **584**, 373 (2020).
- [17] K. Misaki and N. Nagaosa, *Phys. Rev. B* **103**, 245302 (2021).
- [18] M. Rymarz, S. Bosco, A. Ciani, and D. P. DiVincenzo, *Phys. Rev. X* **11**, 011032 (2021).
- [19] H. Wu, Y. Wang, Y. Xu, P. K. Sivakumar, C. Pasco, U. Filippozzi, S. S. Parkin, Y.-J. Zeng, T. McQueen, and M. N. Ali, *Nature (London)* **604**, 653 (2022).
- [20] B. Pal, A. Chakraborty, P. K. Sivakumar, M. Davydova, A. K. Gopi, A. K. Pandeya, J. A. Krieger, Y. Zhang, M. Date, S. Ju *et al.*, *Nat. Phys.* **18**, 1228 (2022).
- [21] J. Díez-Mérida, A. Díez-Carlón, S. Yang, Y.-M. Xie, X.-J. Gao, J. Senior, K. Watanabe, T. Taniguchi, X. Lu, A. P. Higginbotham *et al.*, *Nat. Commun.* **14**, 2396 (2023).
- [22] C. Baumgartner, L. Fuchs, A. Costa, S. Reinhardt, S. Gronin, G. C. Gardner, T. Lindemann, M. J. Manfra, P. E. Faria Junior, D. Kochan *et al.*, *Nat. Nanotechnol.* **17**, 39 (2022).
- [23] K.-R. Jeon, J.-K. Kim, J. Yoon, J.-C. Jeon, H. Han, A. Cottet, T. Kontos, and S. S. Parkin, *Nat. Mater.* **21**, 1008 (2022).
- [24] N. F. Q. Yuan and L. Fu, *Phys. Rev. B* **98**, 045103 (2018).
- [25] Y.-M. Xie, D. K. Efetov, and K. T. Law, *Phys. Rev. Res.* **5**, 023029 (2023).
- [26] See Supplementary Material at <http://link.aps.org/supplemental/10.1103/PhysRevLett.130.266003> for (1) scattering matrix method for the 1D toy model, (2) JDE in TBG with unconventional pairing, (3) the tight-binding model for TBG, (4) Josephson current in the valley-polarized Chern insulator phase of TBG, and (5) JDE in Rashba wire with antisymmetric spin-orbit coupling, which includes Refs. [27–34].
- [27] M. Oh, K. P. Nuckolls, D. Wong, R. L. Lee, X. Liu, K. Watanabe, T. Taniguchi, and A. Yazdani, *Nature (London)* **600**, 240 (2021).
- [28] F. Wu, A. H. MacDonald, and I. Martin, *Phys. Rev. Lett.* **121**, 257001 (2018).

- [29] F. Wu and S. Das Sarma, *Phys. Rev. B* **99**, 220507(R) (2019).
- [30] P. M. R. Brydon, D. S. L. Abergel, D. F. Agterberg, and V. M. Yakovenko, *Phys. Rev. X* **9**, 031025 (2019).
- [31] L. Zou, H. C. Po, A. Vishwanath, and T. Senthil, *Phys. Rev. B* **98**, 085435 (2018).
- [32] I. Das, X. Lu, J. Herzog-Arbeitman, Z.-D. Song, K. Watanabe, T. Taniguchi, B. A. Bernevig, and D. K. Efetov, *Nat. Phys.* **17**, 710 (2021).
- [33] B. Lian, Z.-D. Song, N. Regnault, D. K. Efetov, A. Yazdani, and B. A. Bernevig, *Phys. Rev. B* **103**, 205414 (2021).
- [34] L. Fu, *Phys. Rev. Lett.* **103**, 266801 (2009).
- [35] P. Brouwer and C. Beenakker, *Chaos Solitons Fractals* **8**, 1249 (1997).
- [36] H. C. Po, L. Zou, A. Vishwanath, and T. Senthil, *Phys. Rev. X* **8**, 031089 (2018).
- [37] J. Y. Lee, E. Khalaf, S. Liu, X. Liu, Z. Hao, P. Kim, and A. Vishwanath, *Nat. Commun.* **10**, 1 (2019).
- [38] N. Bultinck, S. Chatterjee, and M. P. Zaletel, *Phys. Rev. Lett.* **124**, 166601 (2020).
- [39] J. Liu and X. Dai, *Phys. Rev. B* **103**, 035427 (2021).
- [40] M. Koshino, N. F. Q. Yuan, T. Koretsune, M. Ochi, K. Kuroki, and L. Fu, *Phys. Rev. X* **8**, 031087 (2018).
- [41] S. Pathak, T. Rakib, R. Hou, A. Nevidomskyy, E. Ertekin, H. T. Johnson, and L. K. Wagner, *Phys. Rev. B* **105**, 115141 (2022).
- [42] S. Carr, S. Fang, Z. Zhu, and E. Kaxiras, *Phys. Rev. Res.* **1**, 013001 (2019).
- [43] S. Shapiro, *Phys. Rev. Lett.* **11**, 80 (1963).
- [44] C. Grimes and S. Shapiro, *Phys. Rev.* **169**, 397 (1968).
- [45] S. Mudi and S. Frolov, [arXiv:2106.00495](https://arxiv.org/abs/2106.00495).
- [46] M. J. A. Stoutimore, A. N. Rossolenko, V. V. Bolginov, V. A. Oboznov, A. Y. Rusanov, D. S. Baranov, N. Pugach, S. M. Frolov, V. V. Ryazanov, and D. J. Van Harlingen, *Phys. Rev. Lett.* **121**, 177702 (2018).
- [47] Y. V. Fominov and D. S. Mikhailov, *Phys. Rev. B* **106**, 134514 (2022).
- [48] R. S. Souto, M. Leijnse, and C. Schrade, *Phys. Rev. Lett.* **129**, 267702 (2022).
- [49] J.-X. Lin, P. Siriviboon, H. D. Scammell, S. Liu, D. Rhodes, K. Watanabe, T. Taniguchi, J. Hone, M. S. Scheurer, and J. Li, *Nat. Phys.* **18**, 1221 (2022).
- [50] H. D. Scammell, J. Li, and M. S. Scheurer, *2D Mater.* **9**, 025027 (2022).
- [51] A. Daido, Y. Ikeda, and Y. Yanase, *Phys. Rev. Lett.* **128**, 037001 (2022).
- [52] N. F. Yuan and L. Fu, *Proc. Natl. Acad. Sci. U.S.A.* **119**, e2119548119 (2022).
- [53] J. J. He, Y. Tanaka, and N. Nagaosa, *New J. Phys.* **24**, 053014 (2022).
- [54] H. C. Po, L. Zou, T. Senthil, and A. Vishwanath, *Phys. Rev. B* **99**, 195455 (2019).
- [55] H. Zhou, T. Xie, T. Taniguchi, K. Watanabe, and A. F. Young, *Nature (London)* **598**, 434 (2021).
- [56] H. Zhou, T. Xie, A. Ghazaryan, T. Holder, J. R. Ehrets, E. M. Spanton, T. Taniguchi, K. Watanabe, E. Berg, M. Serbyn *et al.*, *Nature (London)* **598**, 429 (2021).
- [57] H. Zhou, L. Holleis, Y. Saito, L. Cohen, W. Huynh, C. L. Patterson, F. Yang, T. Taniguchi, K. Watanabe, and A. F. Young, *Science* **375**, 774 (2022).
- [58] S. C. de la Barrera, S. Aronson, Z. Zheng, K. Watanabe, T. Taniguchi, Q. Ma, P. Jarillo-Herrero, and R. Ashoori, *Nat. Phys.* **18**, 771 (2022).
- [59] Y. Zhang, R. Polski, A. Thomson, É. Lantagne-Hurtubise, C. Lewandowski, H. Zhou, K. Watanabe, T. Taniguchi, J. Alicea, and S. Nadj-Perge, *Nature (London)* **613**, 268 (2023).